Atmos. Meas. Tech. Discuss., 3, 501–529, 2010
www.atmos-meas-tech-discuss.net/3/501/2010/
© Author(s) 2010. This work is distributed under
the Creative Commons Attribution 3.0 License.

Atmospheric Measurement Techniques Discussions

This discussion paper is/has been under review for the journal Atmospheric Measurement Techniques (AMT). Please refer to the corresponding final paper in AMT if available.

Potential for the use of reconstructed IASI radiances in the detection of atmospheric trace gases

N. C. Atkinson[1], F. I. Hilton[1,2], S. M. Illingworth[2], J. R. Eyre[1], and T. Hultberg[3]

[1]Met Office, Fitzroy Road, Exeter, EX1 3PB, UK
[2]Department of Physics and Astronomy, University of Leicester, LE1 7RH, UK
[3]EUMETSAT, Eumetsat-Allee 1, 64295 Darmstadt, Germany

Received: 8 February 2010 – Accepted: 8 February 2010 – Published: 11 February 2010

Correspondence to: N. C. Atkinson (nigel.atkinson@metoffice.gov.uk)

Published by Copernicus Publications on behalf of the European Geosciences Union.

Abstract

Principal component (PC) analysis has received considerable attention as a technique for the extraction of meteorological signals from hyperspectral infra-red sounders such as the Infrared Atmospheric Sounding Interferometer (IASI) and the Atmospheric Infrared Sounder (AIRS). In addition to achieving substantial bit-volume reductions for dissemination purposes, the technique can also be used to generate reconstructed radiances in which random instrument noise has been suppressed. To date, most studies have been in the context of Numerical Weather Prediction (NWP). This study examines the potential of PC analysis for chemistry applications.

A major concern in the use of PC analysis for chemistry has been that the spectral features associated with trace gases may not be well represented in the reconstructed spectra, either due to deficiencies in the training set or due to the limited number of PC scores used in the radiance reconstruction. In this paper we show examples of reconstructed IASI radiances for several trace gases: ammonia, sulphur dioxide, methane and carbon monoxide. It is shown that care must be taken in the selection of spectra for the initial training set: an iterative technique, in which outlier spectra are added to a base training set, gives the best results. For the four trace gases examined, the chemical signatures are retained in the reconstructed radiances, whilst achieving a substantial reduction in instrument noise.

A new regional re-transmission service for IASI is scheduled to start in 2010, as part of the EUMETSAT Advanced Retransmission Service (EARS). For this EARS-IASI service it is intended to include PC scores as part of the data stream. The paper describes the generation of the reference eigenvectors for this new service.

1 Introduction

The IASI instrument (Infrared Atmospheric Sounding Interferometer; Siméoni et al., 1997) on the MetOp-A satellite is a unique instrument for Earth observation (Phulpin et

AMTD

3, 501–529, 2010

al., 2007). Since its launch in 2007, IASI has been used in a wide range of applications, including numerical weather prediction (NWP) (e.g. Hilton et al., 2009a), air quality monitoring and atmospheric chemistry (e.g. Clerbaux, 2009).

For NWP the focus is typically on those spectral channels that give information on atmospheric temperature and humidity profiles, in the carbon dioxide and water vapour absorption bands. To assimilate the radiances from all 8461 IASI channels would be prohibitively expensive computationally, and in any case the full information content of the spectrum is much lower than the number of channels, so a subset of a few hundred channels is often used (Collard, 2007). Timeliness is critical for NWP applications – with global data generally being made available by EUMETSAT within 2 h of the sensing time, and distributed to NWP users via the Global Telecommunications System (GTS) or via the EUMETCast re-transmission service. The GTS data stream comprises a subset of 300 IASI channels whereas the EUMETCast service currently carries all channels and it is up to the user to select those that are required for the application.

For chemistry applications, on the other hand, the requirements tend to be different. Full resolution spectra are needed covering specific spectral regions where trace gas absorption features are found. Timeliness is usually not critical for climatological studies: for example, Clarisse et al. (2009) have recently reported the first IASI-derived measurements of ammonia total column, and have mapped the concentrations over the course of 2008. However, spectra are increasingly processed in near-real time (e.g. George et al., 2009), and in fact near-real time atmospheric chemistry products are becoming more important in the context of the international efforts under the Global Monitoring for Environment and Security (GMES) and Monitoring Atmospheric Composition and Climate (MACC) projects.

One of the tools being investigated by the NWP community in the context of IASI is the use of Principal Component (PC) analysis for the extraction of meteorological signals from the spectra and suppression of random noise (e.g. Antonelli et al., 2004). By representing a spectrum in terms of up to a few hundred PC scores (against a set of reference eigenvectors) instead of 8461 channels, a significant reduction in data vol-

AMTD
3, 501–529, 2010

ume can be achieved. Experiments are being undertaken both in the direct assimilation of PC scores (M. Matricardi, personal communication, 2009) and in the assimilation of radiances reconstructed from the PC scores (Hilton and Collard, 2009b).

PC compression can potentially lead to cost savings in near-real-time data transmission. Motivated by the desire for increased timeliness in IASI data distribution for regional NWP, EUMETSAT are planning a pilot IASI re-transmission service as part of the EUMETSAT Advanced Retransmission Service (EARS) program. For this service it is planned to distribute PC scores, together with raw radiances for selected channels. The same technique may in the future also be used for distribution of the global IASI data – especially after the launch of MetOp-B in 2012, as present communications channels would not be able to accommodate full-resolution data from two IASI instruments without some form of compression.

To date there have been no published studies in the use of IASI PC scores in chemistry applications. A major advantage of the PC technique is its potential to suppress noise, which may provide benefit to the retrieval of chemical species characterised by weak signals. However, there is a concern that the signatures of trace gases may not be retained in the reconstructed spectra. This could occur if the trace gas signal is very weak (significantly below instrument noise level) or if the trace gas signature is not captured in the training set of spectra from which the reference eigenvectors were derived. It is therefore important to understand the implications of PC compression of IASI data for atmospheric chemistry where the use of near-real time data is important.

In this paper we look for the characteristic signatures of some trace gases in IASI reconstructed radiances and compare with the signatures found in the raw radiances. The gases and spectral bands chosen are as follows:

- Ammonia (NH_3) lines in the 850–1000 cm^{-1} region. Ammonia is a short-lived gas emitted primarily from livestock, agriculture and biomass burning (Beer et al., 2008; Clarisse et al., 2009). It is very variable spatially.

- Sulphur dioxide (SO_2) in the 1300–1400 cm^{-1} region. A strong feature found in

AMTD
3, 501–529, 2010

rare events such as volcanic eruptions (Clarisse et al., 2008a)

- Methane (CH_4) in the ν_3 band at 2550–2760 cm^{-1}. Anthropogenic methane sources include rice agriculture, livestock, landfill and biomass burning, with natural sources including wetlands. The ν_3 band band can be used to complement the ν_4 band at 1220–1380 cm^{-1}, as the ν_3 band improves the information in the boundary layer (Razavi et al., 2009).

- Carbon Monoxide (CO) in the 2143–2181 cm^{-1} region. CO is formed during biomass burning, by incomplete combustion of fossil fuels and by oxidation of volatile organic compounds. It has a longer lifetime than NH_3 of a few weeks to months and can be used as a transport tracer.

For each of these trace gases, the use of different sets of reference eigenvectors was examined. The three sets used initially are described in Sect. 2, whilst a fourth is introduced in Sect. 4.

For NH_3, SO_2 and CH_4 we do not attempt to perform any trace gas retrievals from reconstructed radiances, but by identifying the characteristics of the spectra we show the potential for use of the reconstructed radiances in further studies. In the case of CO, we test the effects of PC compression and radiance reconstruction on total column retrievals for an area of enhanced CO over central Africa.

2 PC methodology

For a radiance spectrum $\boldsymbol{x}_i$ (column-vector with m channels at location i), the Principal Component scores, $\boldsymbol{p}_i$ (column-vector rank r where $r \leq m$), are computed from a set of pre-computed eigenvectors, $\mathbf{E}$ (rank $m \times r$), noise normalisation matrix $\mathbf{N}$ ($m \times m$) and a (reference) mean radiance $\overline{\boldsymbol{x}}$:

$$\boldsymbol{p}_i = \mathbf{E}^{\mathbf{T}} \mathbf{N}^{-1} \left(\boldsymbol{x}_i - \overline{\boldsymbol{x}} \right) \quad (1)$$

AMTD
3, 501–529, 2010

The reconstructed radiances, $\boldsymbol{x}'_i$, are given by:

$$\boldsymbol{x}'_i = \mathbf{N}\mathbf{E}\boldsymbol{p}_i + \overline{\boldsymbol{x}} \quad (2)$$

To simplify the computation, the noise normalisation matrix is usually assumed to be diagonal.

The eigenvectors are generated via the covariance matrix, **C**, of the noise-normalised training-set spectra, $\boldsymbol{y}_i$ ($=\mathbf{N}^{-1}\boldsymbol{x}_i$), as described by Collard (2008):

$$\mathbf{C} = \frac{1}{n}\sum_{i=1}^{n}\boldsymbol{y}_i\boldsymbol{y}_i^{\mathsf{T}} - \overline{\boldsymbol{y}}\,\overline{\boldsymbol{y}}^{\mathsf{T}} = \mathbf{E}\boldsymbol{\Lambda}\mathbf{E}^{\mathsf{T}} \quad (3)$$

where n is the number of spectra in the training set, **E** is the matrix of eigenvectors and $\boldsymbol{\Lambda}$ is a diagonal matrix containing eigenvalues. $\overline{\boldsymbol{y}}$ denotes the mean of the n noise-normalised spectra. A software package called the *IASI PCA-based Compression package* is available to allow users to perform this computation, see http://www.nwpsaf.org/.

Equation (3) can in principle yield eigenvectors of rank $m \times m$ – in which case $\boldsymbol{x}'_i$ is identical to $\boldsymbol{x}_i$. However most of the atmospheric signal is contained in a relatively small number of leading eigenvectors, with the lower-order eigenvectors containing mainly instrument noise. Therefore the lower-order eigenvectors are usually discarded.

Three sets of reference eigenvectors were used initially in this study:

1. A set of 150 eigenvectors generated by the Met Office and distributed with the ATOVS and AVHRR Pre-processing Package (AAPP – Atkinson et al., 2008), derived from 6 months of thinned IASI data (15 736 spectra) from July to December 2007. Referred to as *set 1*.

2. A "base" set of eigenvectors generated by EUMETSAT from 74 719 spectra chosen randomly (one per IASI scan line) for 7 different days (7 December 2007, 12 March 2008, 9 May 2008, 26 July 2008, 26 August 2008, 25 September 2008 and 7 January 2009). Each of the three IASI spectral bands is treated separately.

AMTD
3, 501–529, 2010

There are 90 eigenvectors in band 1 (channels 1 to 1997; 645–1144 cm^{-1}), 120 in band 2 (channels 1998 to 5116; 1144.25–1923.75 cm^{-1}) and 80 in band 3 (channels 5117 to 8461; 1924–2760 cm^{-1}). Referred to as *set 2*.

3. As for set 2, but with 6664 "outliers" added to the training set. The outliers are taken from the period 8 to 12 August 2008, which includes the eruption of the Kasatochi volcano in the Aleutian Islands, off south western Alaska. Referred to as *set 3*.

To assess the fit of the reconstructed radiances to the raw radiances, it is useful to compute Reconstruction Scores, R_j, for each spectrum, defined as

$$R_j = \sqrt{\left(\boldsymbol{y}'_j - \boldsymbol{y}_j\right)^{\mathsf{T}} \left(\boldsymbol{y}'_j - \boldsymbol{y}_j\right) \Big/ m} \tag{4}$$

where $\boldsymbol{y}'_j$ is the noise-normalised reconstructed radiance vector for IASI band j, with m channels. The reconstruction scores are typically computed for each of the three IASI spectral bands (corresponding to three physical detectors) in order to detect outlier spectra, although in principle could be tailored to the application and calculated for a wavelength range of interest. Values of R for each band are expected to be close to 1.0 if the reconstructed radiance accurately represents the raw radiance and if the noise profile **N** is realistic (Goldberg et al., 2003).

3 Case studies

3.1 Detection of ammonia

Ammonia has a series of spectral lines in the region 800 to 1200 cm^{-1}. Following Clarisse et al. (2009), we can obtain an indication of the ammonia abundance from the brightness temperature difference between the IASI channel at 867.75 cm^{-1} and two neighbouring window channels, at 861.25 and 873.5 cm^{-1}. We use the case study that

CC BY

is described in detail in Clarisse et al. (2008b) (also in Coheur et al., 2009), in which wildfires close to Greece were observed by IASI in the evening of 25 August 2007.

Figure 1 shows a map of the brightness temperature difference, obtained from raw radiances and from the three varieties of reconstructed radiances described in Sect. 2. The raw radiance map and the reconstructed radiance map obtained from eigenvectors *set 3* match well. The reconstructed radiance signal shows evidence of a lower background noise level, as would be expected. However, the plume feature is significantly attenuated in the reconstructed radiance map obtained from *set 2*, while for *set 1* the feature is almost absent. It must be concluded that the *set 1* and *set 2* training sets do not include sufficient representation of ammonia.

Figure 2 shows difference spectra between a spot inside the plume and a spot on the next IASI scan line which was outside the plume. The positions of the ammonia lines are marked with dashed vertical lines. The *set 3* reconstructed radiances show close agreement with the raw radiances, but the *set 2* and *set 1* plots show reduced ammonia signal. *Set 2* does show the strong lines at 931 and 967 cm^{-1} but even these are greatly attenuated in *set 1*. In order to ascertain whether the poor performance of *set 1* was due to the use of only 150 PCs an experiment was carried out in which the number of PCs was increased to 290. The change made little difference; therefore we conclude that the inability of *set 1* to detect the ammonia signal is due primarily to a lack of significant ammonia episodes within the relatively small *set 1* training set (15 736 spectra).

As a second example, Fig. 3 shows the ammonia signal over northern India on 13 May 2008. This region has been identified by Clarisse et al. (2009) as a persistent source of ammonia, especially during the months May to August. As in the case over Greece, we can see that the raw radiances and the reconstructed radiances give a very similar geographical distribution for the ammonia signal, but the reconstructed radiances (*set 3*) contain a lower level of random noise.

In order to identify the reason why eigenvector *set 3* performs better than *set 2*, the individual spectra in the "outliers" training set were examined for ammonia signals. It

AMTD
3, 501–529, 2010

was found that there were a small number of spectra in eastern Kazakhstan with very high band 1 reconstruction scores (up to 3.2). This is one of the ammonia hot-spot regions reported by Clarisse et al. (2009). Clearly the inclusion of these outliers is adding an ammonia signal to the eigenvectors.

Looking more closely at the eigenvectors themselves, the ammonia signal was found to be most obvious in the band 1 eigenvectors of rank 38 and 40, as shown in Fig. 4. Note that there are 90 eigenvectors in band 1, so the ammonia signal is by no means one of the weakest signals to be included – implying that on the rare occasions that the signal is present, it is well above instrument noise.

3.2 Detection of volcanic SO_2

The characteristics of SO_2 spectra are described in detail by Clarisse et al. (2008a). There are two bands that can be detected by IASI, the ν_1 band centred on 1150 cm^{-1} and the ν_3 band centred on 1360 cm^{-1}. According to Clarisse et al. the ν_1 band is difficult to use because of an ice signature and emissivity features on arid land, therefore we concentrate on the ν_3 band. This is within IASI band 2. Following Clarisse et al., we identify major concentrations of SO_2 by measuring the brightness temperature difference between two channels in the absorption band (1371.5 and 1371.75 cm^{-1}) and two "baseline" channels (1407.25 and 1408.75 cm^{-1}).

Figure 5 shows a map of the SO_2 signal on 8 August 2007 in the vicinity of the Kasatochi eruption, for raw radiances and the three varieties of reconstructed radiances. As in the ammonia cases, the reconstructed radiances from the *set 3* eigenvectors give good agreement with the raw radiances. The *set 2* eigenvectors significantly over-estimate the signal, whereas the *set 1* eigenvectors significantly under-estimates the signal. Difference spectra (inside the plume minus outside) are shown in Fig. 6.

The band 2 reconstruction scores using the two sets of EUMETSAT eigenvectors are shown in Fig. 7. The reduction in reconstruction error for the *set 3* eigenvectors is clear, though there is still some residual structure. The removal of this residual structure is

AMTD
3, 501–529, 2010

discussed in Sect. 4.

Because some of the Kasatochi outliers were included in the training set for *set 3*, the analysis was repeated for an independent case – the eruption of Jebel at Tair (30 September 2007), described in Clarisse et al. (2008a). The results (not shown) were very similar to the Kasatochi case, with good agreement between the *set 3* reconstructed spectra and the raw spectra. As before, the *set 2* eigenvectors significantly over-estimated the signal and the *set 1* eigenvectors under-estimated the signal.

3.3 Detection of methane in the short-wave band

As mentioned in Sect. 1, the methane short-wave v_3 band can be used to improve methane retrievals in the boundary layer – complementing the long-wave v_4 band. During the day the solar radiation reflected by the Earth's surface increases the IASI signal substantially in the short-wave band. However, at night, or if the reflected solar radiation is low, the signal to noise ratio (SNR) can be very poor. Razavi et al. (2009) found that it was necessary to improve the SNR in order to perform satisfactory retrievals of CH_4, even during the day: to do this they averaged four contiguous IASI measurements (50×50 km).

Reconstructed radiances could be used to improve the SNR, and hence reduce the need to perform spatial averaging. This is illustrated in Fig. 8, which shows raw and reconstructed brightness temperature spectra for a night-time case, using the *set 3* eigenvectors. The improved SNR for the reconstructed spectrum is striking, with the methane (and HDO) signatures clearly visible.

3.4 Retrieval of carbon monoxide

The impact of PC compression on the retrieval of carbon monoxide from IASI observations has been investigated using an algorithm that is under development at the University of Leicester (Illingworth et al., 2010). This retrieval scheme uses an optimal estimation method (Rodgers, 2000), with the Oxford Reference Forward Model (RFM), to

AMTD
3, 501–529, 2010

retrieve tropospheric columns of CO from IASI measured radiances. RFM is based on the line-by-line model GENLN2 (Edwards, 1992). Unlike the other gases that are under investigation, the CO retrieval does not use a simple differencing technique, so we have tested the impact of the use of reconstructed radiances on the retrievals themselves, using PC scores calculated from *set 1* and *set 3* eigenvectors. The retrieval scheme makes use of the spectral interval 2143–2181 cm^{-1} which contains 10 CO lines.

Figure 9 shows raw and reconstructed spectra using *set 3* eigenvectors and the difference between them, for one observation with enhanced CO. The reconstructed spectrum is extremely close to the raw data in this spectral region. There is no marked correspondence between the differences and the location of the CO lines in general, although the spectra do differ at 2162 cm^{-1}, close to the centre of a CO absorption line. Furthermore, the differences seen in this spectral band for this observation are much smaller than some of those seen in the CH_4 case (Fig. 8).

Figure 10 shows retrievals for clear sky observations from 1 April 2008 over the Congo river basin and southern Cameroon from raw IASI radiances, *set 1* and *set 3* reconstructed radiances. Enhanced CO levels are observed in the North of the area of study. The retrievals from the reconstructed radiances are similar to those from the raw radiances. *Set 1* retrievals show some small differences in the tropospheric column amount, but the overall pattern of high and low retrieved values corresponds well. The *set 3* retrievals seem to show a slightly more coherent pattern of high retrieved CO for the northernmost points, but are otherwise very similar. Figure 11 shows the difference in retrieved CO for *set 3* eigenvectors, and retrieved CO for raw radiances, plotted as a fraction of the estimated total column retrieval error. The differences between raw and *set 3* radiances produce differences in retrieved values which are generally less than 50% of the retrieval error.

One way in which the performance of a retrieval scheme can be assessed is in terms of the fit of the retrieved quantities to the data used in the retrieval. Figure 12 shows the average residual fit to IASI of the forward-modelled CO retrievals from Fig. 10. In both cases, the residual fit is within the instrument noise across the spectral region,

AMTD
3, 501–529, 2010

indicating that the principal component compression has had no major effect on the behaviour of the retrieval scheme. The *set 1* residuals (not shown) were slightly worse, going outside instrument noise for two channels, which is indicative of a poor retrieval for some footprints. This is in keeping with the results for the other trace gases which indicated that the *set 1* eigenvectors performed less well than *set 3* for trace gases associated with biomass burning.

4 Further refinement of the eigenvectors

The previous section has shown that the set of eigenvectors generated through the addition of outliers to the initial training set generally performs well. However, close examination of the reconstruction scores showed that there was still scope for improvement. Therefore to generate a set of eigenvectors for operational use, further iterations were carried out. The process involved the addition of further outlier spectra to the training set – identified through the reconstruction scores, and also through more detailed examination of reconstruction errors in specific parts of the IASI spectrum. The aim of this process is to minimize the number of spectra with anomalously high reconstruction scores.

At the same time the noise normalisation matrix, **N**, was refined. Starting with the IASI noise covariance from CNES as a first guess, a refined noise estimate was computed by adding the covariance of the residuals to the estimate of the noise covariance retained in the reconstructed radiances. Two iterations were used. The use of eigenvectors based on the new noise normalisation led to reduced spatial correlation of the residuals: spatial correlations would imply the presence of scene structure that is not being represented in the reconstructed radiances.

The training set from which the final set of eigenvectors was generated comprises the following data:

– The base set of 74 719 spectra, selected from 7 days of IASI data (see Sect. 2).

CC BY

Having selected the base set, the noise normalisation matrix was computed, as described above.

- 26 150 outlier spectra selected from 12 months of IASI data. An iterative procedure was used in which the eigenvectors were re-computed as further sets of outliers were identified; 7 iterations were used.
- A further 960 outlier spectra selected from 15 months of IASI data, using the thresholds 1.2, 1.25 and 1.45 in the reconstruction scores for the three bands. Care was taken to exclude anomalous spectra resulting from instrument mode transitions, and also to exclude anomalous spectra associated with the South Atlantic Anomaly.

Figure 13 shows the band 1 reconstruction scores for the biomass burning plume presented in Fig. 1 – comparing the scores from the new set of eigenvectors (*set 4*) with those from *set 3*. The new set is much more homogeneous than the old set (noting the expanded scale), and the mean reconstruction score is very close to 1.0, confirming that the new estimate for the noise covariance is more accurate than the old.

It is proposed to use this new set of eigenvectors in the pre-operational EARS-IASI system. Further updates can be considered if the initial evaluation of the EARS-IASI data shows that an update is desirable. An updated version of the AAPP package will allow users to read the eigenvectors and readily generate reconstructed radiances (Atkinson et al., 2009).

5 Conclusions

Principal component compression allows IASI spectra to be disseminated and archived efficiently and additionally reduces the amount of random instrument noise in the reconstructed spectra considerably. The case studies in this paper have shown that trace

AMTD
3, 501–529, 2010

gas signals can be retained in the reconstructed spectra, and their signal-to-noise ratios can be enhanced, but it is very important that the training set used in the generation of the eigenvectors contains adequate representation of rare events.

Random selection of the training set spectra (as was used in the eigenvectors currently distributed with AAPP) does not adequately represent rare events such as biomass burning or volcanic eruptions. Moreover it does not capture the more persistent but geographically limited ammonia emissions associated with agriculture. However, an iterative procedure, involving refinement of a base training set by the addition of outlier spectra, is successful. The final set of eigenvectors, described in Sect. 4, will be used in the EARS-IASI system.

Whilst the qualitative results shown in this paper are very encouraging for PC reconstructions, it is recommended that more detailed and quantitative studies are carried out into trace gas retrievals using reconstructed radiances.

References

Antonelli, P., Revercomb, H. E., Sromovsky, L., Smith, W. L., Knuteson, R. O., Tobin, D. C., Garcia, R. K., Howell, H. B., Huang, H.-L., and Best, F. A.: A principal component noise filter for high spectral resolution infrared measurements, J. Geophys. Res., 109, D23102, doi:10.1029/2004JD004862, 2004.

Atkinson, N. C., Brunel, P., Marguinaud, P., and Labrot, T.: AAPP developments and experiences with processing METOP data, Tech. Proc, 16th Int. TOVS Study Conf., Angra dos Reis, Brazil, 6–13 May, 2008.

Atkinson, N. C., Ponsard, C., and Hultberg, T.: AAPP enhancements for the EARS-IASI service, Proc. EUMETSAT Meteorological Satellite Conf., Bath, UK, 21–25 September, 2009.

Beer, R., Shephard, M. W., Kulawik, S. S., Clough, S. A., Eldering, A., Bowman, K. W., Sander, S. P., Fisher, B. M., Payne, V. H., Luo, M., Osterman, G. B., and Worden, J. R.: First satellite observations of lower tropospheric ammonia and methanol, Geophys. Res. Lett., 35, L09801, doi:10.1029/2008GL033642, 2008.

Clarisse, L., Coheur, P. F., Prata, A. J., Hurtmans, D., Razavi, A., Phulpin, T., Hadji-Lazaro, J., and Clerbaux, C.: Tracking and quantifying volcanic SO_2 with IASI, the September 2007

AMTD
3, 501–529, 2010

eruption at Jebel at Tair, Atmos. Chem. Phys., 8, 7723–7734, 2008a, http://www.atmos-chem-phys.net/8/7723/2008/.
Clarisse, L., Coheur, P.-F., Hurtmans, D., Clerbaux, C., Turquety, S., and Hadji-Lazaro, J.: IASI measurements of Trace Species and Particles in Volcanic and Fire Plumes, ACCENT-TROPOSAT-2 Activities 2007–2008 and Final Report, 82–86, 2008b.
Clarisse, L., Clerbaux, C., Dentener, F., Hurtmans, D., and Coheur, P.-F.: Global ammonia distribution derived from infrared satellite observations, Nat. Geosci., 2, 479–483, 2009.
Clerbaux, C., Boynard, A., Clarisse, L., George, M., Hadji-Lazaro, J., Herbin, H., Hurtmans, D., Pommier, M., Razavi, A., Turquety, S., Wespes, C., and Coheur, P.-F.: Monitoring of atmospheric composition using the thermal infrared IASI/MetOp sounder, Atmos. Chem. Phys., 9, 6041–6054, 2009, http://www.atmos-chem-phys.net/9/6041/2009/.
Coheur, P.-F., Clarisse, L., Turquety, S., Hurtmans, D., and Clerbaux, C.: IASI measurements of reactive trace species in biomass burning plumes, Atmos. Chem. Phys., 9, 5655–5667, 2009, http://www.atmos-chem-phys.net/9/5655/2009/.
Collard, A. D.: Selection of IASI channels for use in numerical weather prediction, ECMWF Tech. Memorandum 532, 2007.
Collard, A. D.: NWPSAF ECMWF IASI PCA-Based Compression Package Manual, NWP SAF document NWPSAF-EC-UD-011, online available at: http://www.nwpsaf.org/, 2008.
Edwards, D. P.: GENLN2: A general line-by-line atmospheric transmittance and radiance model, NCAR Tech.Note, NCAR/TN-367+STR, 1992.
George, M., Clerbaux, C., Hurtmans, D., Turquety, S., Coheur, P.-F., Pommier, M., Hadji-Lazaro, J., Edwards, D. P., Worden, H., Luo, M., Rinsland, C., and McMillan, W.: Carbon monoxide distributions from the IASI/METOP mission: evaluation with other space-borne remote sensors, Atmos. Chem. Phys., 9, 8317–8330, 2009, http://www.atmos-chem-phys.net/9/8317/2009/.
Goldberg, M. D., Qu, Y., McMillin, L. M., Wolf, W., Zhou, L., and Divakarla, M.: AIRS near- real-time products and algorithms in support of operational numerical weather prediction, IEEE T. Geosci. Remote Sens., 41, 379–389, 2003.
Hilton, F., Atkinson, N. C., English, S. J., and Eyre, J. R.: Assimilation of IASI at the Met Office and assessment of its impact through observing system experiments, Q. J. Roy. Meteorol. Soc., 135, 495–505, 2009a.

Hilton, F. and Collard, A. D.: Recommendations for the use of principal component-compressed observations from infrared hyperspectral sounders, Met Office Forecasting Research and Development Technical Report 536, online available at: http://www.metoffice.gov.uk/research/nwp/publications/papers/technical{_}reports/, 2009b.

Illingworth, S. M., Remedios, J. J., Boesch, H., Moore, D. P., Sembhi, H., Dudia, A., and Walker, J. C.: An Optimal Estimation retrieval scheme for carbon monoxide over a localised region using the IASI instrument, in preparation, 2010.

Phulpin, T., Blumstein, D., Prel, F., Tournier, B., Prunet, P., and Schlussel, P.: Applications of IASI on MetOp-A: first results and illustration of potential use for meteorology, climate monitoring, and atmospheric chemistry, proc. SPIE, 6684, 66840F, 2007.

Razavi, A., Clerbaux, C., Wespes, C., Clarisse, L., Hurtmans, D., Payan, S., Camy-Peyret, C., and Coheur, P. F.: Characterization of methane retrievals from the IASI space-borne sounder, Atmos. Chem. Phys., 9, 7889–7899, 2009, http://www.atmos-chem-phys.net/9/7889/2009/.

Rodgers, C.: Inverse Methods for Atmospheric Sounding: Theory and Practice, World Scientific, 2000

Siméoni, D., Singer, C., and Chalon, G.: Infrared atmospheric sounding interferometer, Acta Astronautica, 40, 113–118, 1997

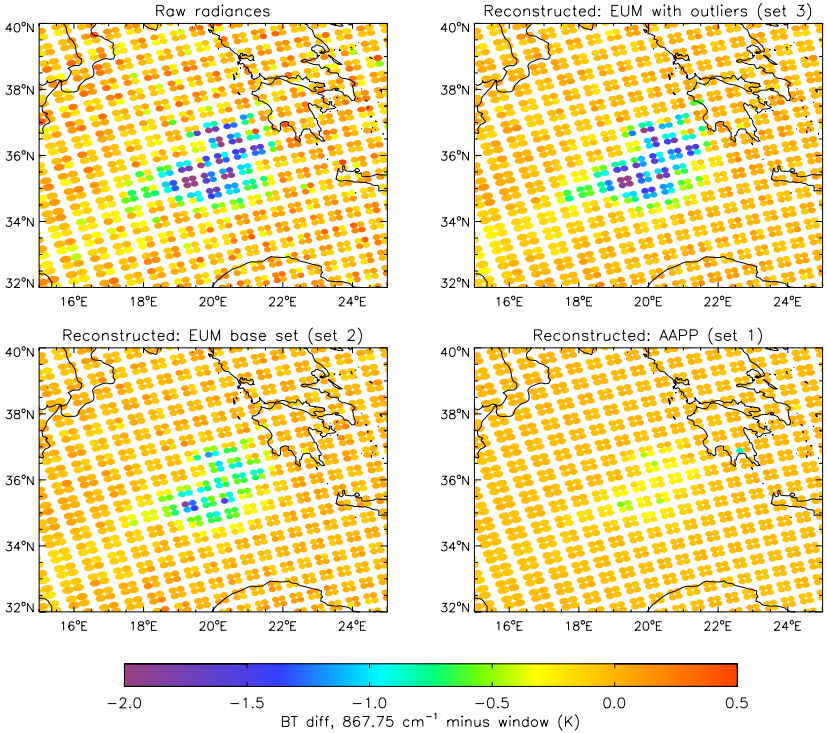

Fig. 1. Ammonia signal associated with biomass burning near Greece on 25 August 2007, 19:38 MetOp overpass. The brightness temperature at 867.75 cm^{-1} has been subtracted from the brightness temperature in adjacent window channels. Shown for raw radiances and three varieties of reconstructed radiances. The BT scale has been fixed at −2.0 to +0.5 K in order to show background noise, but it should be noted that the strongest signal was −3.7 K. For display purposes, the size of the IASI spots has been increased from 12 km at nadir to 20 km in order to show colours clearly.

AMTD
3, 501–529, 2010

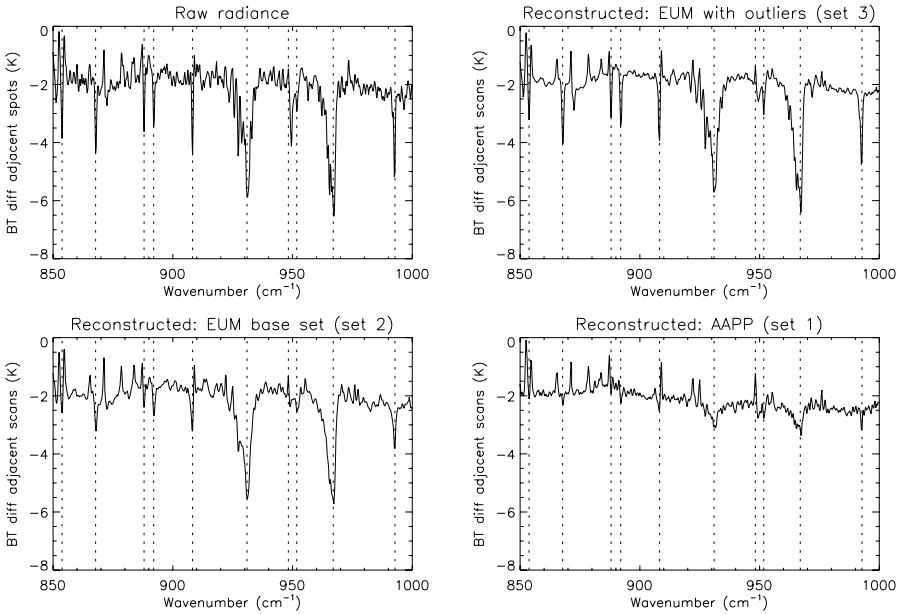

Fig. 2. Difference spectra between a spot on the northern edge of the plume and a spot on the following IASI scan line which is outside the plume. Vertical dotted lines mark the positions of ammonia absorption lines, from Clarisse et al., 2008b. Other spectral features unrelated to ammonia also appear more clearly in the reconstructed spectra.

AMTD
3, 501–529, 2010

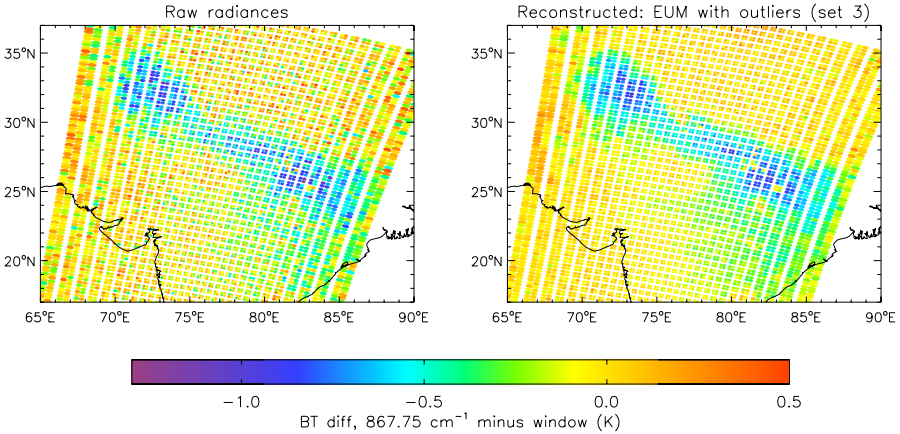

Fig. 3. Ammonia signal associated with agriculture over northern India. 13 May 2007, morning overpass.

AMTD
3, 501–529, 2010

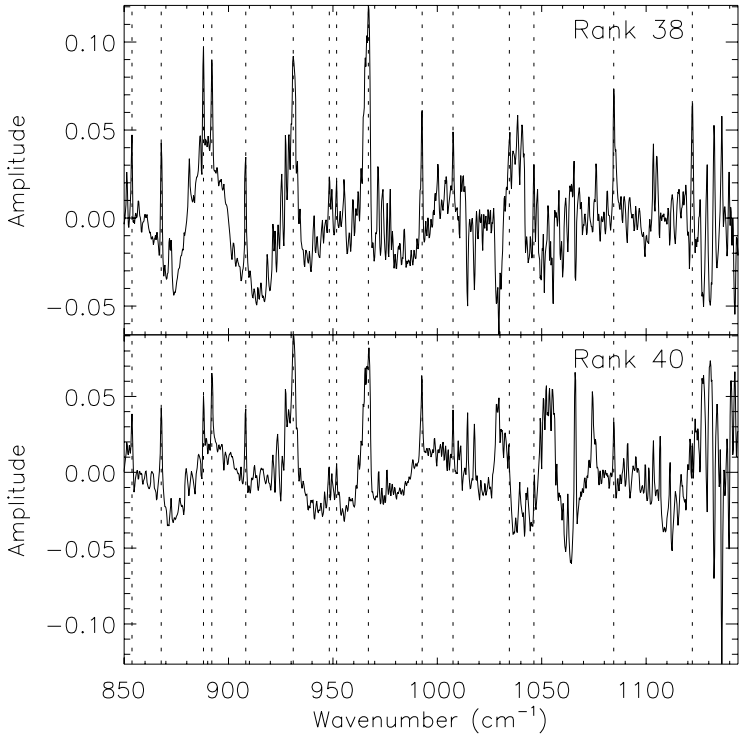

Fig. 4. Eigenvectors of rank 38 and 40 in IASI band 1. Both contain a strong signature of ammonia. Vertical lines mark the ammonia absorption lines, from Clarisse et al., 2008b.

AMTD
3, 501–529, 2010

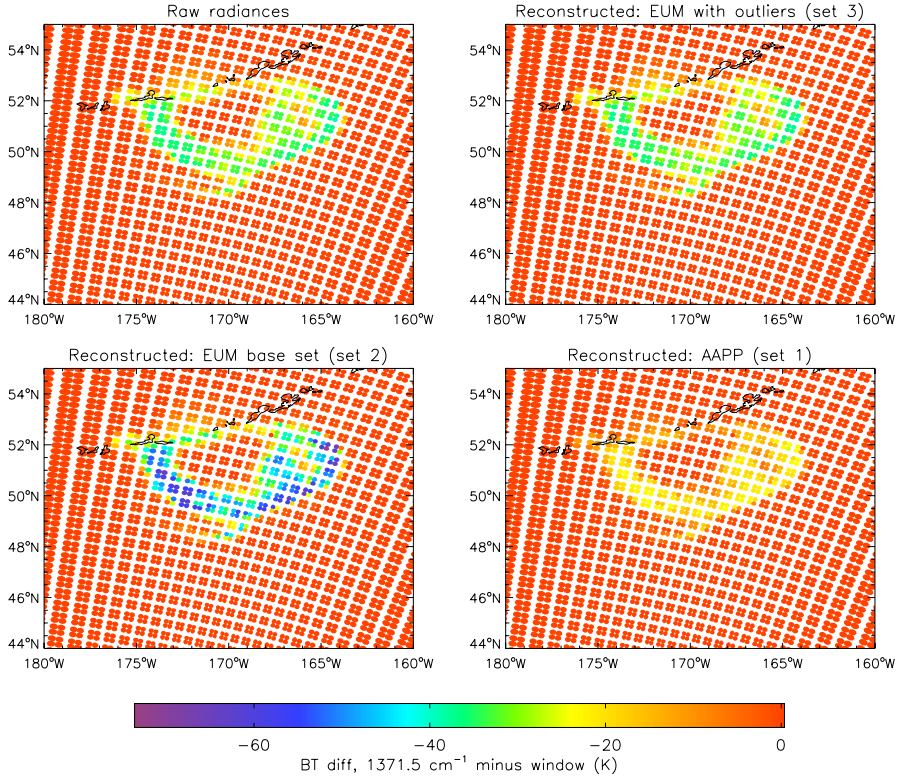

Fig. 5. SO_2 signal associated with the Kasatochi volcano eruption on 8 August 2008, 21:23 MetOp overpass. The brightness temperature at 1371.5 and 1371.75 cm^{-1} has been subtracted from the brightness temperature in adjacent window channels. Note the anomalously large signal in the reconstructed radiances from the *set 2* eigenvectors. The volcano is located at 52.18° N, 175.5° W.

AMTD
3, 501–529, 2010

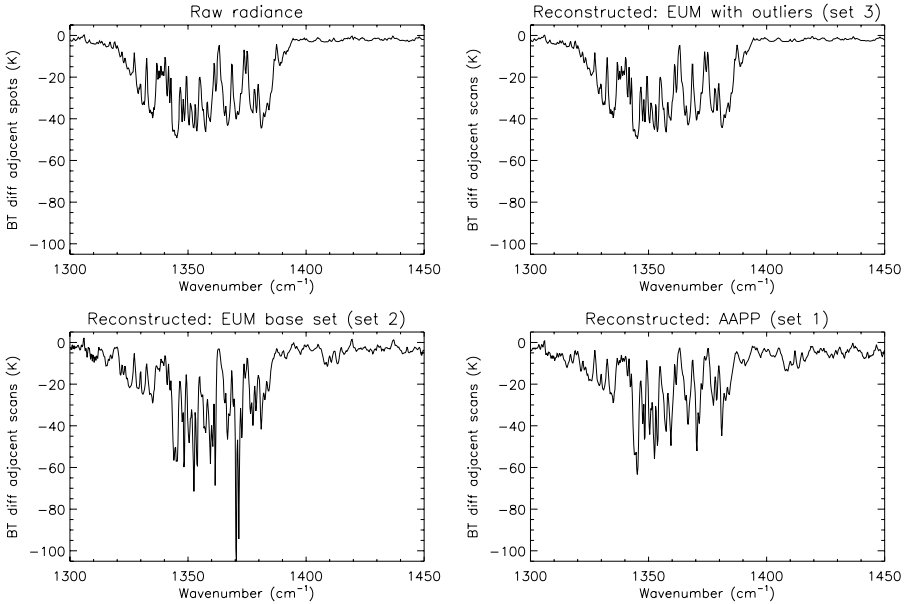

Fig. 6. Difference spectra between a spot on the north-eastern edge of the Kasatochi plume and a spot on the previous IASI scan line which is outside the plume. The ν_3 band of SO_2 covers the range 1320 to 1400 cm^{-1}.

AMTD
3, 501–529, 2010

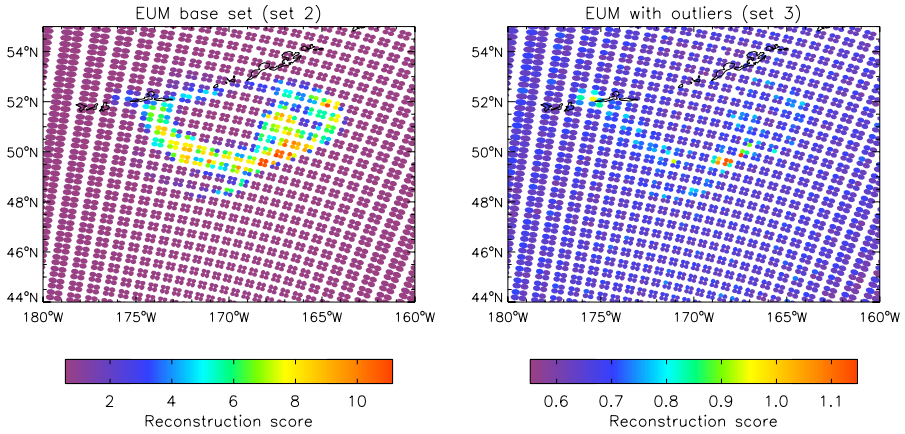

Fig. 7. Band 2 reconstruction scores for the Kasatochi eruption, showing the improvement in scores when outliers are included in the PC training set.

AMTD
3, 501–529, 2010

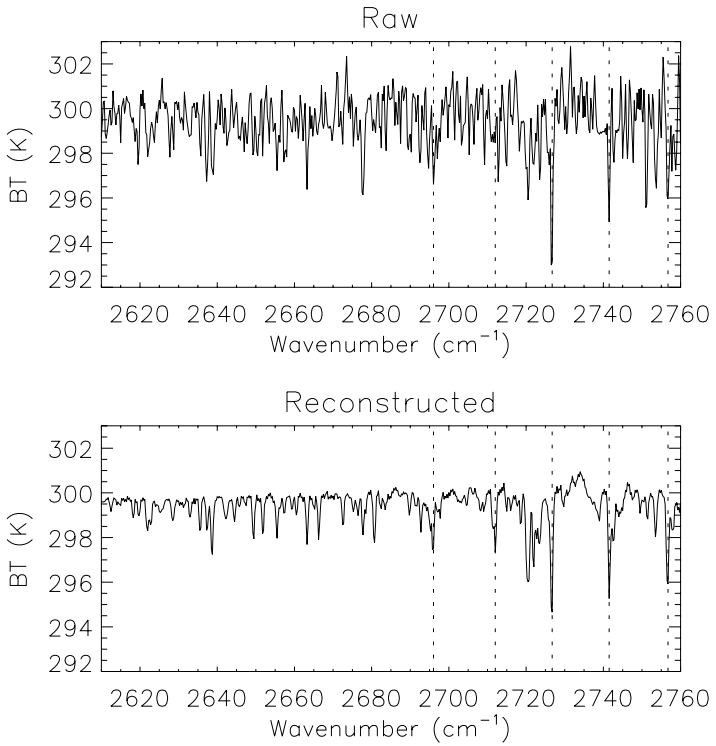

Fig. 8. Raw and reconstructed brightness temperature spectra showing methane lines in IASI band 3, for a night-time overpass. Vertical dotted lines mark the positions of methane absorption lines, from Razavi et al., 2009. The other spectral lines in the 2620 to 2690 cm^{-1} range (and also at 2720 cm^{-1}) are HDO. Data taken from 25 August 2007, 19:38 MetOp overpass, over the Mediterranean (same case as Fig. 1, but well away from the biomass burning plume).

AMTD
3, 501–529, 2010

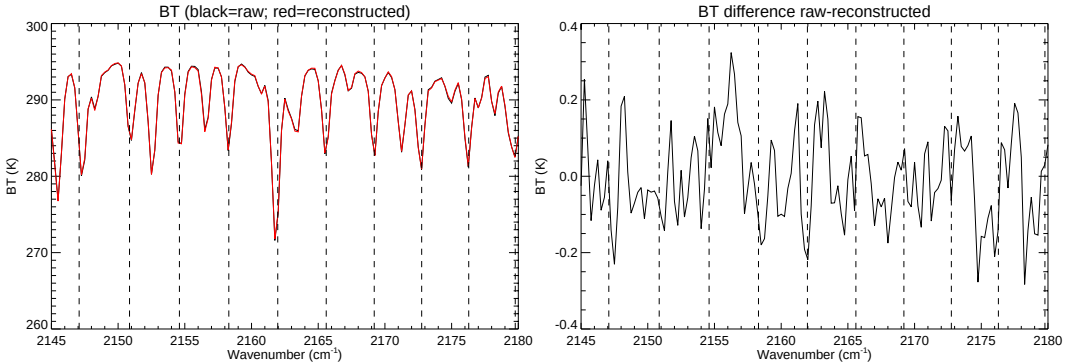

Fig. 9. Raw and reconstructed brightness temperature spectra (left) and the difference between them (right) for an enhanced CO observation. *Set 3* eigenvectors were used. CO absorption lines are marked with vertical dashed lines.

AMTD
3, 501–529, 2010

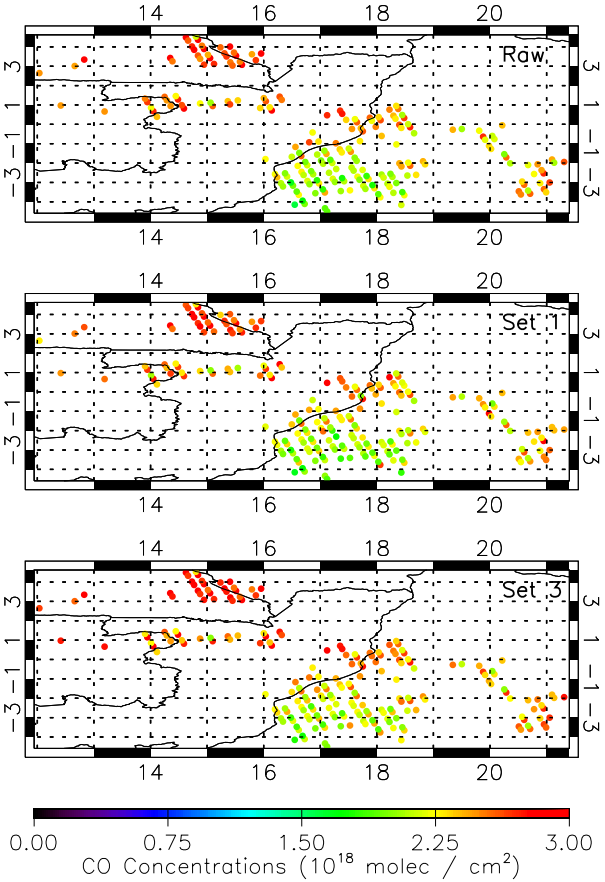

Fig. 10. Total column CO retrievals for 1 April 2008 over West Central Africa using IASI raw radiances (top), *set 1* eigenvectors (middle) and *set 3* eigenvectors (bottom).

AMTD
3, 501–529, 2010

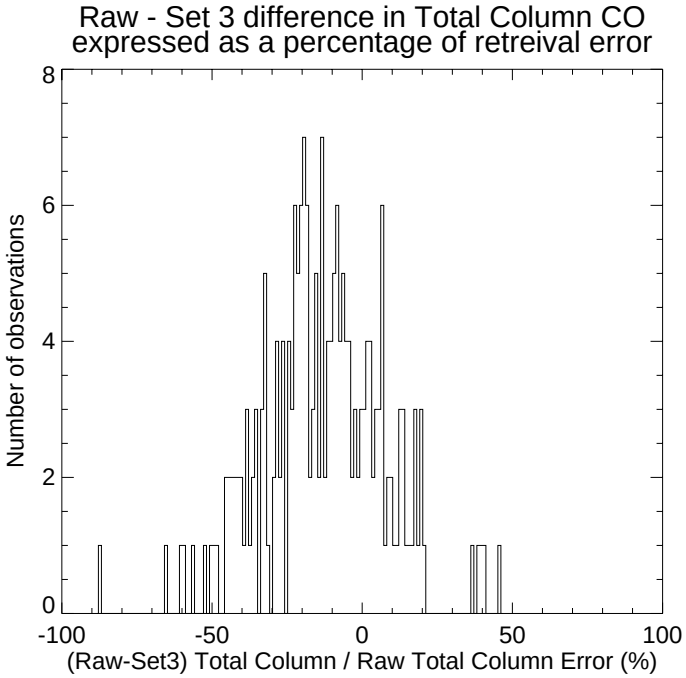

Fig. 11. Difference in total column CO amount retrieved from *set 3* eigenvectors and raw radiances, expressed as a fraction of retrieval error.

AMTD
3, 501–529, 2010

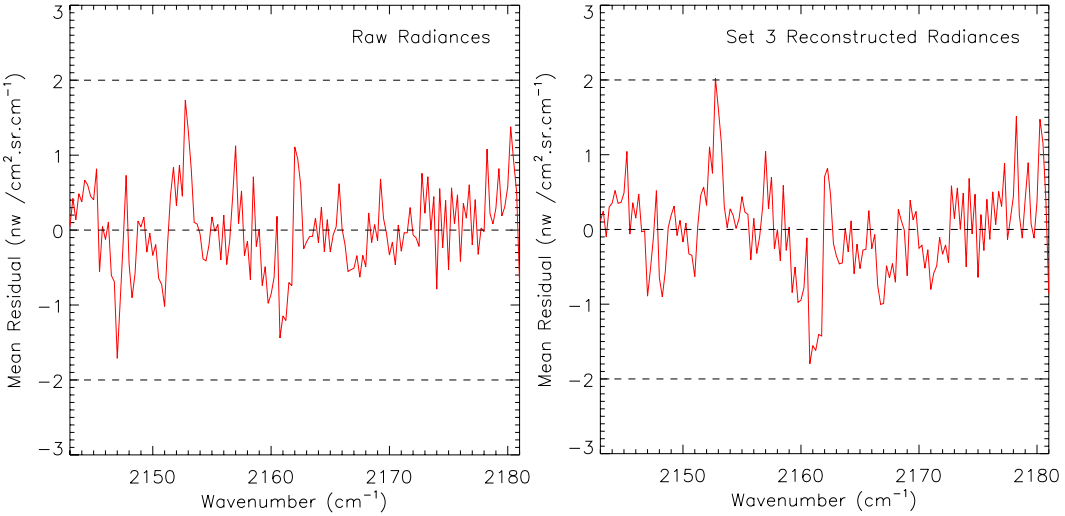

Fig. 12. Mean residual fit to IASI observations from all footprints in Fig. 10 for the raw radiances (left) and for the set 3 reconstructed radiances (right). The dashed lines show the instrument noise level.

AMTD
3, 501–529, 2010

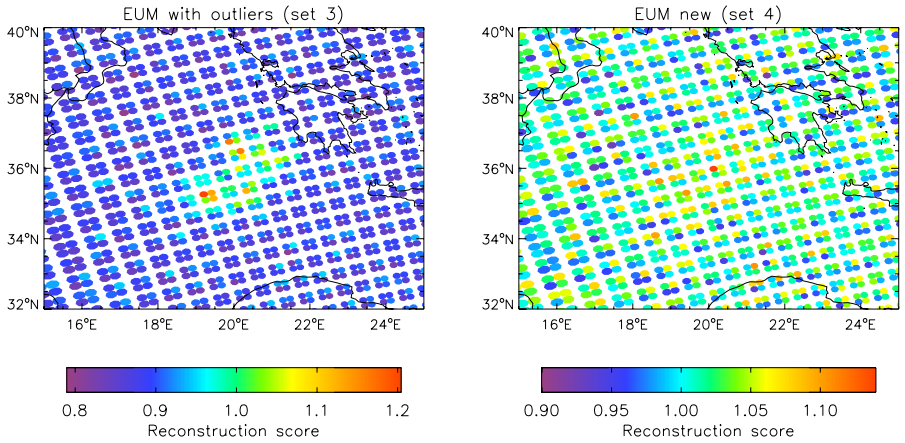

Fig. 13. Band 1 reconstruction scores for the case presented in Fig. 1, showing the improvement in homogeneity when the new set of EUMETSAT eigenvectors is used (see Sect. 4). Note the expanded scale in the right hand plot, allowing the background variability outside the biomass burning plume to be seen.

AMTD
3, 501–529, 2010